Fourier, Fresnel and Image CGHs of three-dimensional objects observed from many different projections

David Abookasis and Joseph Rosen
Ben-Gurion University of the Negev
Department of Electrical and Computer Engineering
P. O. Box 653, Beer-Sheva 84105, Israel

ABSTRACT

We describe new techniques of synthesizing three types of computer-generated hologram (CGH); Fourier, Fresnel and image CGHs. These holograms, aimed to reconstruct three-dimensional (3-D) objects, are synthesized by means of a unique algorithm of fusing multiple perspective views of the observed scene. The hologram is initially generated in the computer as a Fourier hologram. Then, it can be converted to either Fresnel or image holograms by computing the desired wave propagation and the interference process. By illuminating the ready-to-use CGHs with a collimated plane wave, a 3-D image of the objects is reconstructed. Diffraction efficiency enhancement of the above algorithm by superimposing a random phase on the object during the CGH formation is also presented. Computer simulation and experimental results of the constructed 3-D objects demonstrate the suggested technique.

Keywords: Computer Holography, Fourier CGH, Fresnel CGH, Image CGH, Multiple Projections.

1. INTRODUCTION

Synthesizing a computer-generated hologram (CGH) of a three-dimensional (3-D) image can be a heavy computational task[1]. One needs to superpose the mathematical contributions of many waves originating from many points on the objects, when not all of them are located at the same distance from the hologram plane. Recently[2] we have developed a new procedure for generating a CGH of general 3-D objects by fusing multiple angular projections of computer-designed objects. By performing a data reduction in a specific computation process on the entire set of angular perspectives of the 3-D object, a single 2-D complex function is obtained representing the wavefront distribution on the hologram plane. This complex function is then conventionally encoded to a CGH with real and positive transparency values. Illuminating the CGH by a plane wave constructs an image of the original object with the desired 3-D cues. This method reduces the amount of computing operations to that of a CGH of 2-D objects, and more important, it enables synthesizing a hologram of both realistic[3] or computer-made[2,4] 3-D objects. Therefore, in some cases this technique can replace the complicated interferometric process of hologram recording. It has been shown[2,3] that merging angular projections together in this technique yields a Fourier hologram equivalent to the well-known optical Fourier hologram[5] recorded by a coherent light source. In this study the procedure of computing a hologram is extended in order to create other types of CGHs.

There are several types of holograms, among them are the three well-known types; Fourier, Fresnel and image holograms[6]. The differences between these holograms are manifested by the different optical setups placed between the object and the hologram plane. A Fourier hologram of a 3-D object is defined as a hologram, located at the back focal plane of a spherical lens, and exposed to a wave coming from an object located at the vicinity of the front focal plane. A Fresnel hologram is formed from an object located within a Fresnel region (in which the Fresnel diffraction formula[6] is satisfactorily valid) from the recording medium. Recently a Fresnel CGH of computer-generated objects from a

series of projections has been suggested.[4] In the present study we extend this work and demonstrate two types of Fresnel CGH. The image hologram is obtained when the optical setup images an object on the hologram plane. Image hologram is positioned inside the volume occupied by the 3-D image, such that the resulting image appears to float in space at the hologram plane. Parts of the image extend forwards from the hologram and other parts remain inside the hologram. The generation of image CGH of 3-D objects, by a different algorithm than described here, has been proposed by Leseberg[7]. Our image CGH is formed from a single Fourier wavefront of the 3-D object in two steps. First the 3-D image is digitally created from the Fourier wavefront. Then, equivalently to the optical interference process, the image is superposed with a digital reference wave.

A critical factor limiting the amplitude computer-generated, and optical, holograms is their inherent low diffraction efficiency. Such efficiency is not tolerable for many practical applications. Therefore, in addition to the above mentioned CGHs, we revisit the topic of Fourier CGH, but at this time the diffraction efficiency is considered. The improved diffraction efficiency is achieved by multiplying the object with a random phase function. Consequently, the spatial spectrum of the modified object spreads more uniformly over the entire spectral region. This technique is effective only because the phase distribution of the reconstructed image is not detectable by the viewer eyes. However introducing random phase on the objects causes to intensity fluctuations (speckles) on the image which might damage the smooth texture of the reconstructed image.[8]

2. ALGORITHM FOR MAKING 3D CGH USING MULTIPLE POINT OF VIEW

Before describing the various types of CGHs, we briefly summarize the algorithm for synthesizing Fourier CGH from multiple perspectives, first presented in Ref. 2, and shown in Fig. 1.

The first step in the algorithm is to generate a 3-D object in the computer memory. Next, the set of the object's angular projections are computed. Then, each projection is multiplied by a corresponding phase function and the product is summed to a single complex value. The end product of the process is a single two-dimensional complex function representing the wavefront distribution on the hologram plane. Every complex value in this function is computed from a different angular projection and is positioned in the same order of observing the projected images. The mathematical expression of $s(m,n)$, a single complex value in the wavefront matrix, is given by:

$$s(m,n) = \iint p_{mn}\left(x_p, y_p\right) \exp\left[-j2\pi b(x_p \sin \varphi_m + y_p \sin \theta_n)\right] dx_p dy_p, \qquad (1)$$

where $P_{mn}(x_p,y_p)$ is the m,n-th projected perspective image viewed from the angles φ_m, θ_n in the horizontal and vertical directions, respectively. (x_p, y_p) is the coordinate system of each projection, and b is some real-valued constant. Finally, the complex matrix is coded to a real and positive-valued matrix in order to be used as a holographic transparency. The complete computational process is illustrated schematically below in Fig. 1.

In Ref. 2 we have shown that the above algorithm generates a single complex function $s(m,n)$ equal to the wavefront on the Fourier plane sampled in the m,n points. Therefore, the resulting CGH is equivalent to an optical Fourier hologram of a realistic 3-D scene recorded by a coherently illuminated system. Next we propose a method which enhances the diffraction efficiency of these Fourier CGHs.

3. FOURIER, FRESNEL AND IMAGE CGHs

In this section we describe the three types of CGH mentioned above. In principle, once we have the Fourier wavefront distribution, other CGHs are obtained by computing the propagation of the wavefront from the Fourier plane to any other desired plane.

3A. *Fourier CGH*

As mentioned in the previous section, our algorithm creates a single complex function $s(m,n)$ from the entire projections sets. We have shown in Ref. 2 that this complex function in continuous coordinates (u,v) is related to the 3-D object function $t(x_s, y_s, z_s)$ by the following relation,

$$s(u,v) \propto \iiint t(x_s, y_s, z_s) \exp \left\{ -j \cdot 2\pi \cdot b \left[ux_s + vy_s + a \cdot z_s \cdot (u^2 + v^2) \right] \right\} dx_s\, dy_s\, dz_s \qquad (2)$$

where a, b are some specific constants. Eq. (2) actually describes the wavefront distribution $s(u,v)$ on the back focal plane obtained from coherently illuminated 3-D object positioned in the vicinity of the front focal point and described by the function $t(x_s, y_s, z_s)$.
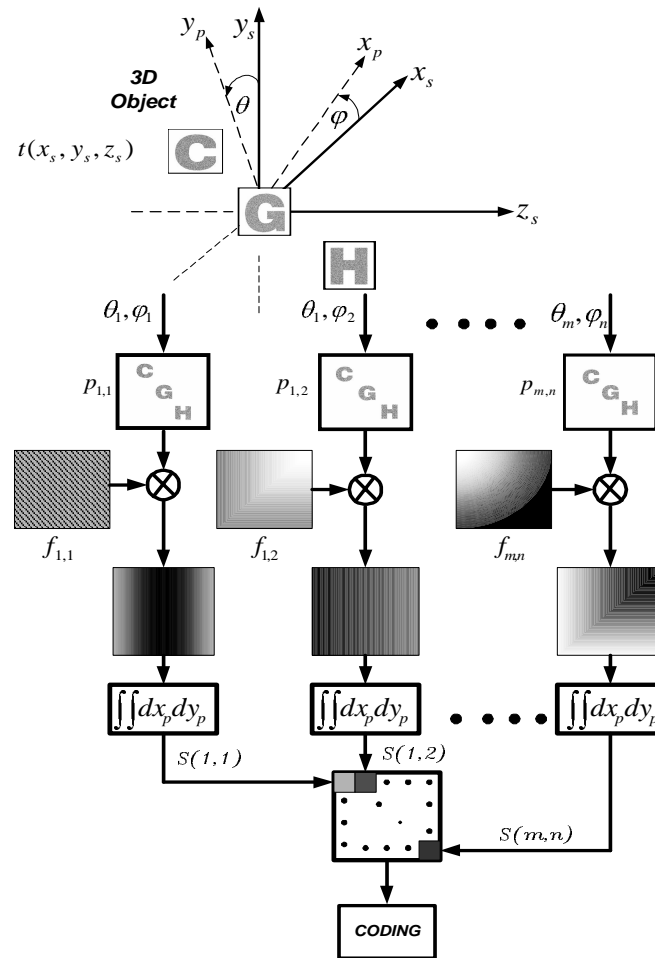

Figure 1: CGH algorithm. $\quad f_{m,n} = \exp\left[-j2\pi b\left(x_p \sin \varphi_m + y_p \sin \theta_n \right) \right].$

Therefore $s(u,v)$ is equivalent to Fourier hologram recorded by a coherently illuminated system but with a 3-D object as the system's input.

In order to improve the diffraction efficiency the magnitude distribution on the hologram plane should be more uniform. In this study we increase the uniformity of the hologram magnitude by multiplying the object function with a random phase. Accordingly, the distribution of the wavefront on the hologram plane can be expressed by

$$s(u,v) \propto \iiint t(x_s, y_s, z_s) \times \exp\left[j\phi(x_s, y_s, z_s) \cdot \xi\right] \exp\left\{-j \cdot 2\pi \cdot b\left[ux_s + vy_s + a \cdot z_s \cdot \left(u^2 + v^2\right)\right]\right\} dx_s dy_s dz_s, \qquad (3)$$

where $\phi(x_s, y_s, z_s)$ is the random phase uniformly distributed between $\pm\pi$. ξ is the randomization factor $0 \leq \xi \leq 1$, which control the influence of the random phase and consequently the uniformity of the spectrum on the hologram plane. In analog to optical holography this factor acts like using different diffuser function.

3B. *Fresnel CGH*

Since the resulting hologram $s(u,v)$ is equivalent to the wavefront on a Fourier plane, it is possible to create a Fresnel hologram by computing the propagation of the wavefront from the Fourier plane to any other desired plane. According to the Fresnel diffraction equation the complex amplitude $U(x_o, y_o)$ on the plane located a distance z from the an aperture with a complex amplitude $t(x_o, y_o)$ is

$$U_O(x_O, y_O) = t(x_O, y_O) * h_z(x_O, y_O) = \Im^{-1}\left\{T(u,v) \cdot H_z(u,v)\right\} \qquad (4)$$

where the symbol * stands for the 2-D linear convolution operator, $h_z(x_o, y_o)$ is the point-spread function (PSF) of the free space given by $h_z(x,y) = \exp[j(\pi/\lambda z)(x^2 + y^2)]$ and $\Im^{-1}$ is the inverse Fourier transform operator. $T(u,v)$ and $H_z(u,v)$ are the Fourier transform of $t(x_o, y_o)$ and $h_z(x_o, y_o)$ respectively. In order to get the desired Fresnel hologram, the Fourier spectrum of the object with is multiplied by a quadratic phase function $H_z(u,v)$ and by linear phase function $R(u,v) = R_o \cdot \exp(j2\pi \alpha v)$. The real part of the inverse Fourier transform of the product yields the desired Fresnel hologram of type I, as follows,

$$I(u,v) = \Re e\left\{s(u,v) \cdot H_z(u,v) \cdot R(u,v)\right\} \qquad (5)$$

where $\Re e$ represents the real part operator. The linear phase function includes the parameter α equal to $\sin(\theta)/\lambda$, where θ is the inclination angle of the first diffraction order. The transverse distance of the reconstructed images from the optical axis is determined by the parameter α according to the following. From the sampling theorem, the hologram with the highest spatial frequency is $f_{max} = 1/2d$ where d is the sampled period. In our hologram the spatial frequency is given by $\alpha = \sin(\theta)/\lambda$. Since $f_{max} = \alpha$ the maximum allowed angle between the object and the reference wave is $\theta = \sin^{-1}(\lambda/2d)$. For $\lambda = 632.8 nm$ and $d = 18\mu m$, the maximum allowed angle is $\theta = 1°48'$.

In the case of Fresnel hologram type-II the procedure is modified such that the reference beam is added digitally to the Fresnel diffraction in a similar manner as in optical holography. The intensity at any point on the hologram plane is given by

$$I(x,y) = \left|u(x,y) + R(x,y)\right|^2 \qquad (6)$$

where $u(x,y)$ is the complex amplitude of the object in the Fresnel region and $R(x,y)$ is the complex amplitude of the reference in (x,y) hologram plane.

3C. *Image CGH*

The last type of hologram we demonstrate in this study is the image hologram. After applying the inverse Fourier transform on the spectrum pattern $s(u,v)$, the image volume is reconstructed in the computer. In the computer we add a reference wave function at the middle plane of reconstructed volume. Consequently, the distribution of the image CGH is given by,

$$I(x_o, y_o) = R_o^2 + \left|\Im\{s(u,v)\}\right|^2 + 2\Re e\left\{R_o \cdot \Im\{s(u,v)\}\exp(j2\pi \cdot \alpha \cdot y_o)\right\} \qquad (7)$$

where $\Im$ is the Fourier transform. According to sub-section 3A α is the spatial frequency corresponding to the oblique angle of the reference. $I(x_o, y_o)$ given by Eq. (7) is a computed transmittance pattern which is later displayed on the

holographic display. The interference term in Eq. (7), which gives the information of the object is $\Im\{s(u,v)\} \cdot \left[R_o \cdot \exp(-j2\pi \cdot a \cdot y_o) \right]$.

4. SIMULATION AND EXPERIMENTAL RESULTS

In the experiment of the Fourier CGH with improved diffraction efficiency, the testing objects were composed from three planar surfaces carrying the letters C, G, H, on each one of them. The 'C' plane was located at the back of the scene at point $(x,y,z)=(-170,170,-170)$ pixels, the 'G' plane was at the center of the scene at point $(x,y,z)=(0,0,0)$ and the 'H' plane was at the front of the scene at point $(x,y,z)=(170, -170, 170)$ pixels. Each letter in the object plane was multiplied by a random phase function. The 3-D scene was observed from an incrementally changed angle from top to bottom in the azimuthal and elevation angles of $\pm10^{o}$, where the angular displacement between every two successive projection was 0.1^{o} in both directions. From 201×201 projections of the 3-D scene, the Fourier hologram pattern was computed according to the procedure sketched in Fig. 1. The central 100×100 pixels of the magnitude of the Fourier hologram compared to the magnitude without the random phase technique are shown in Figs. 2(a) and 2(b), respectively. From these figures it is evident that the spectrum plane in Fig. 2(a) has more uniform magnitude distribution throughout the hologram plane owing to the additional random phase. The simulated reconstruction images from the complex hologram of Figs. 2(a) are shown in Fig. 3. These results were obtained by calculating the diffraction patterns behind a spherical lens at three different transverse planes along the propagation axis z in the vicinity of the rear focal point. These figures show that at each transverse plane, a different letter of different planes is in focus; thus reconstruction of the 3-D objects is demonstrated.
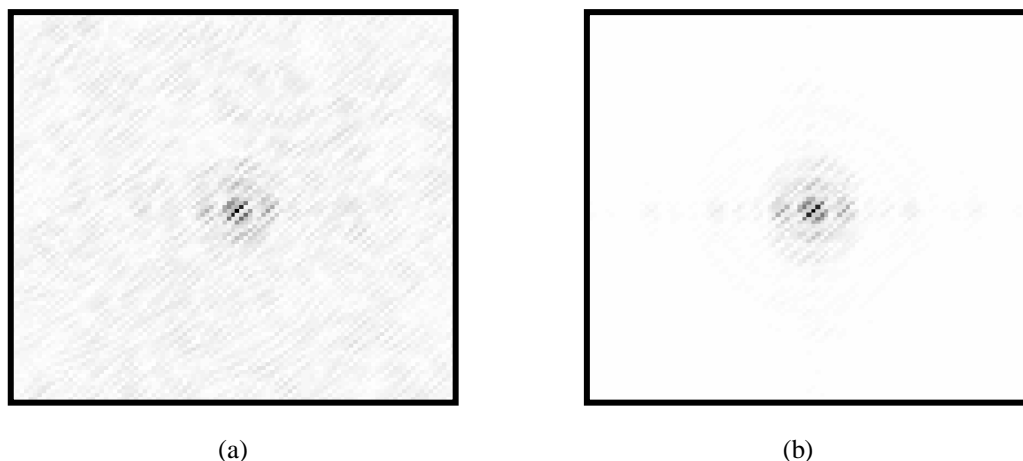

(a)   (b)

Figure 2: Enlarged portion (100×100 pixels of 201×201) of **(a)** the magnitude with random phase and **(b)** without random phase of the CGH generated by the algorithm shown in Fig. 1

To assess the reconstruction quality quantitatively, the normalized mean square error (MSE) and the diffraction efficiency (η) were employed for the three transverse planes in which the three letters are in focus. The diffraction efficiency of a diffractive mask is given by the intensity ratio between the light within the diffraction zone to the illuminating wave. The overall diffraction efficiency was measured from the simulation results and was found to be 0.0103%. In comparison with the hologram obtained from zero phase objects [Fig. 2(b)] where the diffraction efficiency is 0.0016%, the diffraction efficiency has been improved by a factor of six.

An error measure should reflect the similarity between the original object and the reconstructed image. The average MSE was 0.4811% and 0.2308% for the reconstructed images from the holograms in Fig. 2(a) and 2(b), respectively. As expected introducing a random phase function causes of more speckles on the image and therefore the reconstructed error is increased.
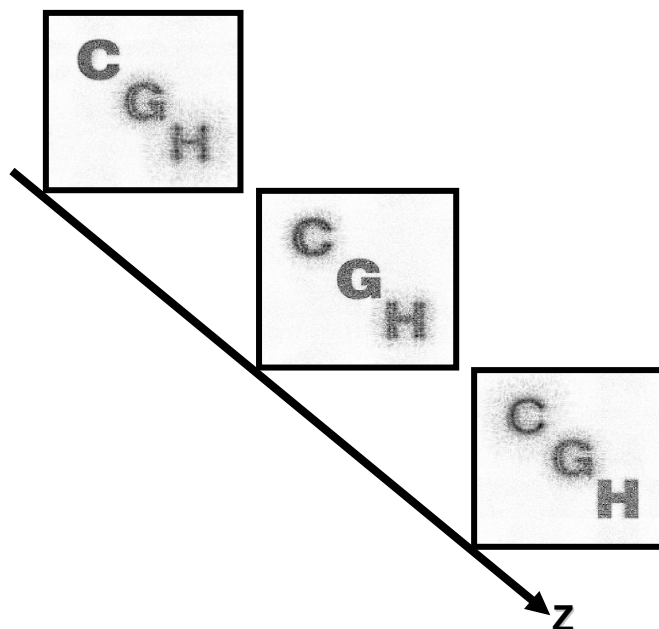

Figure 3: Simulated reconstruction from the hologram shown in Fig. 2(a) at the vicinity of the back focal plane of the Fourier lens for three successive transverse planes along the optical axis.

In the second experiment we synthesized the two-types of the Fresnel hologram discussed in section 3B. In the tested object of the Fresnel CGH type-I the ball with the letter 'C' was at the back of the scene at point $(x,y,z)=(-170,0,-170)$, and the 'H' ball was at the front of the scene at point $(x,y,z)=(170, 0,-170)$. In the case of Fresnel CGH type-II the testing object was composed of three balls carrying the letters C, G, H, located in the same space coordinate as the three planes of the Fourier CGH mentioned above. The difference from the Fresnel hologram type-I is the addition of one more ball between the other two balls, carrying the letter G and located at the center of the scene at point $(x,y,z)=(0,0,0)$. The Fresnel hologram type-I is shown in Fig. 4. The images constructed from the hologram by computer simulation in two transverse planes are depicted in Fig. 5. The hologram pattern and the reconstruction from the Fresnel CGH type-II are shown in Fig. 6 and Fig. 7, respectively. Those figures show that at each transverse plane a different letter of a different ball is in focus, indicating the success of the 3-D construction.

Finally the image CGH is considered. The 3-D object used here was composed of three cubes carrying the letters B, G, U, one on each of them. The 'B' cube was at the back of the scene at point $(x,y,z)=(-125,0,-125)$ pixels, the 'G' cube was at the center of the scene at point $(x,y,z)=(0,0,0)$ and the 'U' cube was at the front of the scene at point $(x,y,z)=(125,0,-125)$ pixels. Each cube has the size of $85\times85\times85$ pixels. As mentioned above the process starts from the algorithm of synthesizing the Fourier CGH. By computing the inverse Fourier transform of the hologram the images of the balls are digitally reconstructed. Then we add a reference wave in the computer and get the desired image hologram, shown in Fig. 8. The object reconstruction along the propagation axis z at three different locations with respect to the hologram plane is shown in Fig. 9.
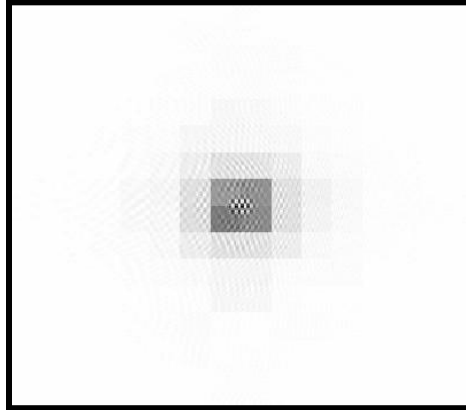
Figure 4: Enlarged portion (300x300 pixels of 600x600) of the color inverted intensity distribution
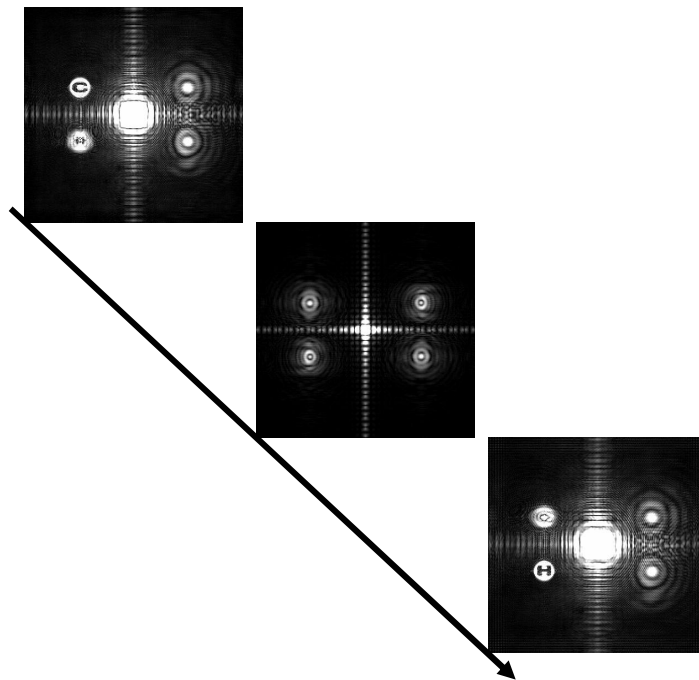of the Fresnel CGH type-I.

Figure 5: Digitally reconstruction images from the hologram of Fig. 4 along the optical axis.

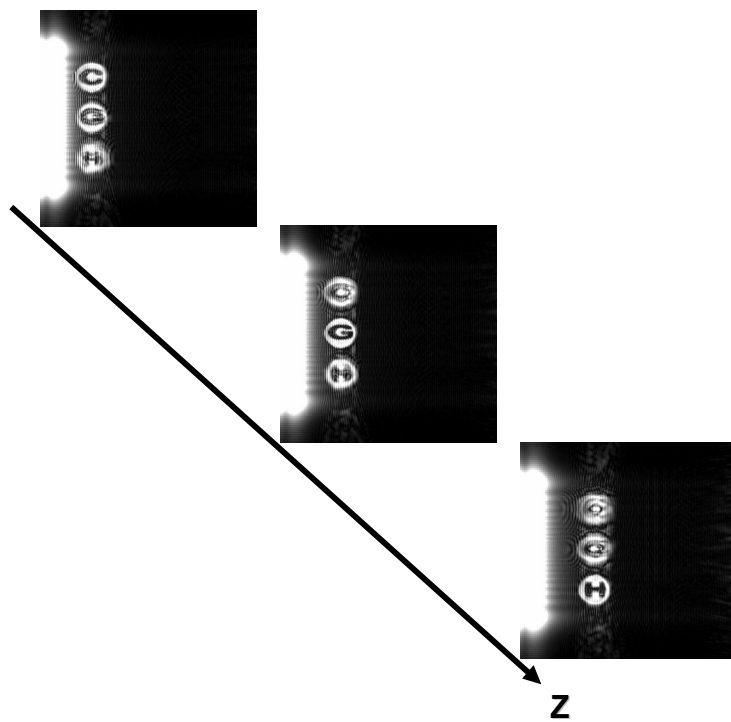Figure 6: Enlarged portion of the intensity distribution of the Fresnel CGH type-II.

Figure 7: Digitally reconstructed images from Fig. 6 for three successive transverse planes along the optical axis.
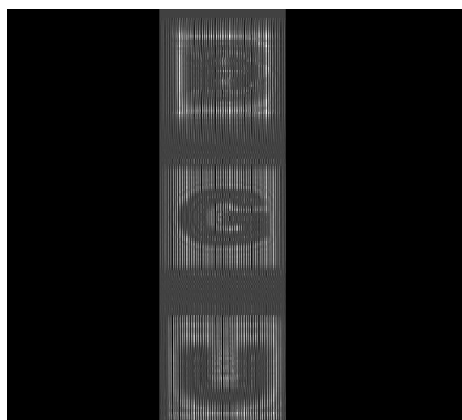
Figure 8: Enlarged portion of the intensity distribution of the Image CGH.
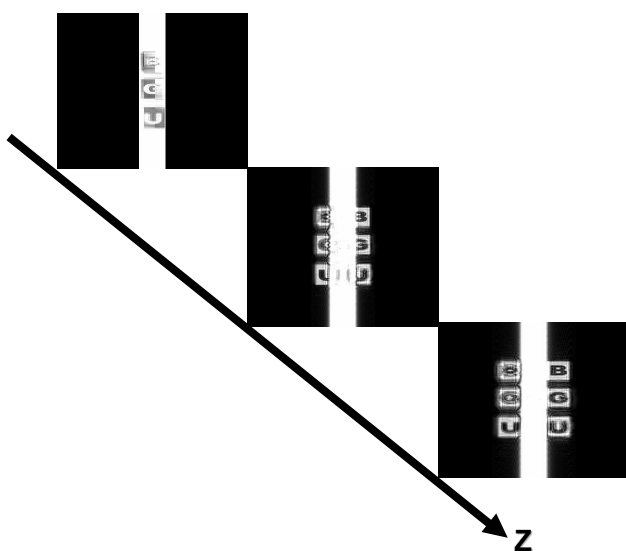

Figure 9: Digitally reconstructed images from Fig. 8 for three successive transverse planes along the optical axis.

To observe the holographic reconstruction we illuminated the four computed CGHs displayed on an SLM (CRL, Model XGA3) with a collimated beam emerging from a He-Ne laser radiating at 632.8nm. Several experiments were conducted to verify the above-mentioned concept. The entire types of holograms were encoded into positive, real valued function in order to be displayed on the SLM. The parameter b (see Ref. 2) in these experiments was chosen to be equal to 0.9. The reconstruction results in the vicinity of the back focal plane of the Fourier lens (f=750mm) are shown in the Fig. 10. The entire pictures were captured with an 8-bit 795×596 pixels CCD at three different transverse planes along the optical axis; 733, 762, and 790mm from the lens. The distance between the lens and the SLM was 75mm.
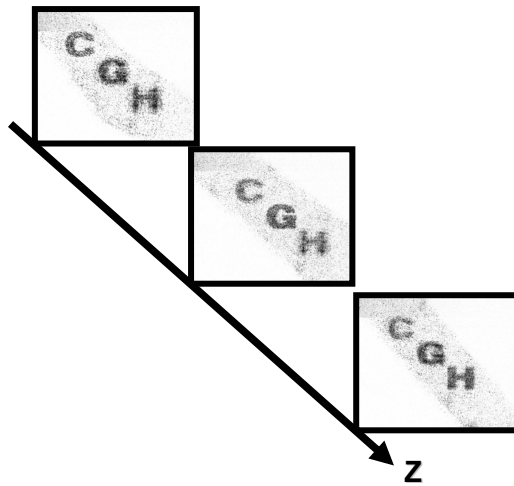
Figure 10: Optical reconstruction of the hologram shown in Fig. 2(a) in the vicinity of the back focal plane at distances of 733 mm, 762 mm, and 790 mm from the lens. The contrast in these figures has bee inverted for better visualization.

For reconstructing both types of Fresnel CGH, the reconstructed plane was shifted closer to the hologram plane by using a spherical lens (f=400mm). Fig. 11 shows the Fresnel CGH type-I and the reconstruction results observed by the CCD obtained at two different distances from the lens. The 'C' ball and the 'H' ball were obtained at 525mm and 565mm from the lens, respectively. Fig. 12 shows the reconstruction of the Fresnel CGH type-II at 740, 780 and 810mm from the lens for 'C', 'G', 'H' balls, respectively. In both experiments the distance between the lens and the SLM was 140mm.
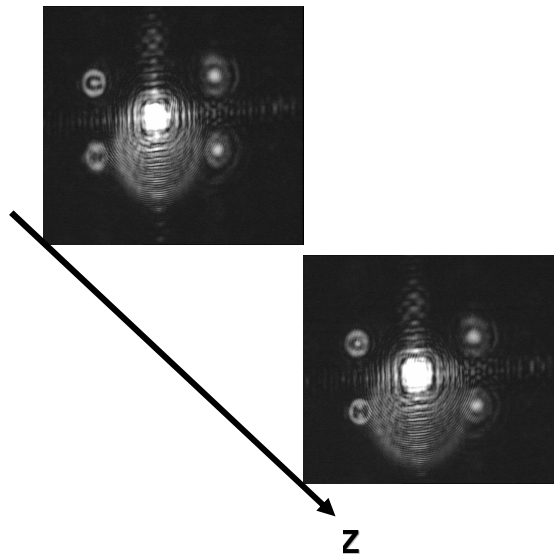

Figure 11: Optical reconstruction of Fig. 4 (Fresnel CGH type-I) in the vicinity of the back of the lens, for two transverse planes at 525mm and 565 mm.
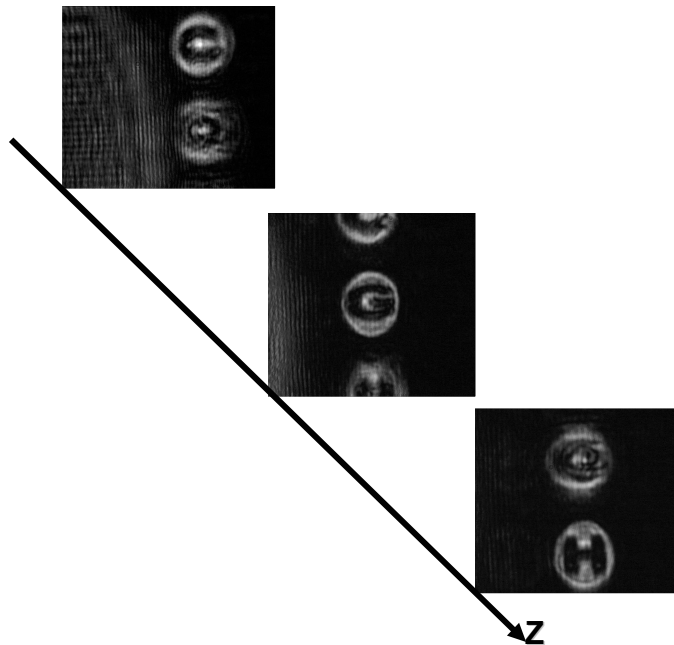
Figure 12: Optical reconstruction of Fig. 6 (Fresnel CGH type-II) in the vicinity of the back of the lens, for three transverse planes at 740mm, 780 mm and 810mm.

The reconstruction results of the image CGH without any lens between the hologram and the observer are shown in Fig. 13(a) while in 13(b) we used an imaging lens (f=400mm) only for improving the visualization. The distance between the lens and the SLM was 120mm.
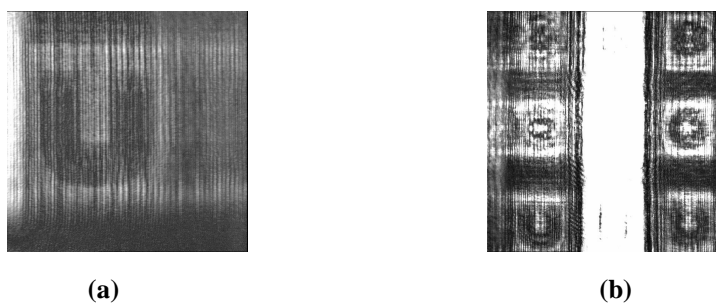

(a)

(b)

Figure 13: Optical reconstruction of the Image hologram shown in Fig. 8, (a) the 'H' cube at 605mm and (b) 320mm from the SLM and using imaging lens.

5. DISCUSSION AND CONCLUSION

From the entire reconstruction results we see that parts of the objects are in focus, while others parts appear out of focus. This feature creates the desired illusion of an object with a sizeable volume. We also see that the optical results agree with the theory and with the simulation results. The loss of quality in the pictures of the optical reconstruction is due to experimental difficulties such as non-uniform illumination, noise introduced by the optical elements, and the poor quality of the SLM.

In conclusion, we have presented and successfully demonstrated the evaluation of a new process for computing CGHs of the types Fourier, Fresnel and image holograms. A 2-D complex function is obtained from multiple view projections of a 3-D object. This function contains the 3-D information of the object and it is related to the object's Fourier transform. Consequently, we succeeded in creating Fresnel and image CGHs by using the Fresnel diffraction equations. Multiplying the object by a random phase during the CGH creation increases both the diffraction efficiency and unfortunately also the noise on the reconstructed images. These methods have a high potential in versatile holographic applications such as 3-D cameras and displays.

REFERENCES

1. C. D. Cameron, D. A. Pain, M. Stanley and C. W. Slinger, "Computational challenges of emerging novel true 3D holographic displays," *SPIE* **4109,** 129-140, 2000.
2. D. Abookasis and J. Rosen, "Computer-generated holograms of three-dimensional objects synthesized from their multiple angular viewpoints," *J. Opt. Soc. Am. A* **28**, 1537-1545, 2003.
3. Y. Li, D. Abookasis, and J. Rosen, "Computer-generated holograms of three-dimensional realistic objects recorded without wave interference," *Appl. Opt.* **40**, 2864-2870, 2001.
4. Y. Sando, M. Itoh, and T. Yatagai, "Holographic three-dimensional display synthesized from three-dimensional Fourier spectra of real existing objects," *Opt. Lett* **28**, 2518-2520, 2003.
5. A. B. VanderLugt, "Signal detection by complex spatial filtering," *IEEE Trans. Inf. Theory* **IT-10**, 139–145, 1964.
6. A. P. Hariharan, *Optical Holography*, 2nd ed. (Cambridge New York 1996), Chap. 2, pp. 19-21.
7. D. Leseberg, "Computer-generated three-dimensional image holograms," *Appl. Opt.* **31,** 223–229, 1992.
8. J. W. Goodman, *Introduction to Fourier Optics,* 2nd ed. (McGraw-Hill, New York, 1996), Chap. 6, 158-160.